One-step model of photoemission from single-crystal surfaces

Siddharth Karkare, Weishi Wan, and Jun Feng
Lawrence Berkeley National Laboratory, 1 Cyclotron Rd., Berkeley, California 94720, USA

Tai C. Chiang
Department of Physics and Frederick Seitz Materials Research Laboratory, University of Illinois, Urbana, Illinois 61801, USA

Howard A. Padmore
Lawrence Berkeley National Laboratory, 1 Cyclotron Rd., Berkeley, California 94720, USA
(Received 22 December 2016; revised manuscript received 27 January 2017; published 28 February 2017)

In this paper, we present a three-dimensional one-step photoemission model that can be used to calculate the quantum efficiency and momentum distributions of electrons photoemitted from ordered single-crystal surfaces close to the photoemission threshold. Using Ag(111) as an example, we show that the model can not only calculate the quantum efficiency from the surface state accurately without using any *ad hoc* parameters, but also provides a theoretical quantitative explanation of the vectorial photoelectric effect. This model in conjunction with other band structure and wave function calculation techniques can be effectively used to screen single-crystal photoemitters for use as electron sources for particle accelerator and ultrafast electron diffraction applications.

DOI: 10.1103/PhysRevB.95.075439

I. INTRODUCTION

Over the past few decades photoemission based tools such as photoelectron spectroscopy (PES) and angle-resolved photoelectron spectroscopy have proven extremely successful in studying the chemical and electronic structure of solid state materials and surfaces [1]. As a result, physics of the photoemission phenomena has been well investigated with regard to explaining the angle-resolved electron energy spectra obtained using UV and x-ray light sources.

More recently, photoemission has gained popularity as a source of electrons for several applications such as free electron lasers (FELs) [2] and ultrafast electron diffraction (UED) [3] experiments. The quantum efficiency (QE) and the transverse (to the normal on the photoemission surface) momentum spread or the rms transverse momentum are the most critical figures of merit of the photoemission based electron sources (or photocathodes) that limit the performance of such applications [4]. For example, the transverse coherence length of the electron beam in UED which limits the largest lattice size that can be studied is inversely proportional to the rms transverse momentum of electrons emitted from the cathode [5]. The transverse momentum spread also limits the smallest possible electron beam emittance which defines the shortest possible lasing wavelength of an FEL [6]. The QE determines the drive laser power needed to obtain the electron bunch charge required for the particular application; a low QE can imply high drive laser power often making the drive laser system prohibitively complex and expensive [7]. High drive laser power can also limit the smallest possible rms transverse momentum through ultrafast laser heating of the electron gas [8]. Hence a high QE is required.

Despite the technological importance of solid state photoemission as an electron source, the physics that governs the relevant photoemission properties of QE and rms transverse momentum is not well understood. Spicer followed the three-step model to first calculate the electron yield from silver and copper surfaces [9]. The first theories to model the rms transverse momentum from photocathodes were formulated by Flottmann [10] and by Jensen *et al.* [11] and followed a three-step photoemission model. Dowell and Schmerge refined these theories and put them on a better foundation [12]. The Dowell and Schmerge formulation successfully explained the QE and rms transverse momentum obtained from polycrystalline or disordered cathodes but did not model photoemission very close to the threshold accurately. An extension to this theory was developed recently, to model photoemission near the threshold [13]. It showed that the smallest possible rms transverse momentum from polycrystalline surfaces is thermally limited by the temperature of the lattice. However these models did not include the effects of band structure, polarization, and angle of incident light (the vectorial photoelectric effect [14,15]) and did not model emission from single-crystal surfaces of metals. A technique to estimate the rms transverse momentum spread from single-crystal faces of metal cathodes using the band structure calculated from density functional theory was developed by Li *et al.* [16]. However, this technique does not estimate the QE and assumes uniform probability of photoemission from any given electron state which is generally not true.

In this paper, we present a scheme to calculate the QE and transverse momentum spread accurately using an one-step photoemission model. Our model is a three-dimensional (3D) expansion of the one-dimensional (1D) photoemission model developed by Miller *et al.* [17,18] to explain ultraviolet photoemission spectra obtained from single-crystal surfaces of noble metals. Photoemission is modeled as a one-step process of the transition of electrons from the initial bulk or surface state (ss) inside the metal to a time-reversed low-energy electron-diffraction (LEED) -like free electron state under the influence of the electromagnetic field of the incident light. We obtain the rate of such a transition using the Fermi golden rule to calculate the QE and the rms transverse momentum of emitted electrons. This photoemission model takes into account the effects of band structure, polarization, and angle of incident light.

Using the (111) surface of silver as an example, we show that our model predicts the QE near threshold accurately and explains the effects of polarization of incident light and angle of incidence quantitatively. We show that the emission from an Ag(111) surface at threshold, at an angle of incidence near 60° is dominated by the electrons emitted from the Shockley surface state [19] resulting in a QE of greater than 5×10^{-5} very close to the photoemission threshold. We also calculate the rms transverse momentum of electrons emitted from the Ag(111) surface. We show that the Ag(111) surface can simultaneously provide a high QE and a low rms transverse momentum very close to the thermal limit [13] and hence can be used as an excellent electron source.

The dependence of QE on the polarization of incident light and angle of incidence is called the vectorial photoelectric effect and has been investigated experimentally, but has been modeled only empirically [14,15]. Using our scheme to calculate the QE we show that the vectorial photoelectric effect results from the variation of the overlap integral with the angle of incidence and polarization of incident light and can be modeled without use of any empirical data [20].

II. THE ONE-STEP MODEL

A. Basic formalism

We assume that the normal to the solid-vacuum interface is along the z direction and the classical interface is located at $z = 0$, with $z > 0$ being the vacuum side. The Hamiltonian of the photon-electron interaction is given by

$$\mathcal{H} = \frac{1}{2m_e}\left(\vec{p} - \frac{e}{c}\vec{A}\right)^2 - \frac{p^2}{2m_e} \tag{1}$$

$$\approx -\frac{e\hbar}{m_e c}\vec{A}\cdot\vec{\nabla} - \frac{e\hbar}{2m_e c}(\vec{\nabla}\cdot\vec{A}), \tag{2}$$

where $\vec{p}$ is the momentum operator, $\vec{A}$ is the vector potential of the incident light, e is the unit charge, c is the speed of light, and m_e is the mass of a free electron in vacuum.

The vector potential of incident light inside the metal surface can be given by $\vec{A} = A_0 e^{([z-z_0)/d_l]}\vec{\epsilon}$, where A_0 is the magnitude of the incident vector potential just outside the surface, $\vec{\epsilon}$ is the polarization vector inside the surface, d_l is the decay length of the incident light in the metal, and z_0 is the location of the interface adjusted to account for the spilling over of the electron cloud into vacuum [17,18] due to the surface state. For the Ag(111) surface z_0 is determined by wave function matching of the Shockley surface state at the solid-vacuum interface as shown in Sec. III B. Note that the magnitude of polarization vector $\vec{\epsilon}$ is not unity and takes into account the reflection at the surface as given in Sec. II B. The incident photon flux per unit area is given by

$$F = \frac{2\varepsilon_0 |A_0|^2 \omega}{\hbar c}\cos(\theta_i), \tag{3}$$

where ω is the frequency of incident light, ε_0 is the dielectric constant of vacuum, and θ_i is the angle of incidence [21].

For ultraviolet light, the wavelength is long enough that the $\vec{\nabla}\cdot\vec{A}$ term in Eq. (2) can be ignored everywhere except at the metal-vacuum interface. At the metal-vacuum interface, there is a sharp discontinuity in $\vec{A}$ in the z direction and $\vec{\nabla}\cdot\vec{A}$ results in a delta function at $z = z_0$. The Hamiltonian is then given by

$$\mathcal{H} = -\frac{e\hbar A_0 e^{z' H(-z')/d_l}}{m_e c}[\vec{\epsilon}\cdot\vec{\nabla} + C\epsilon_z \delta(z')], \tag{4}$$

where ϵ_z is the z component of $\vec{\epsilon}$, $H(z)$ is the Heaviside function, $z' = z - z_0$, and C is a constant that depends only on the photon energy and the properties of the solid. The constant C can be obtained by fitting the calculations of the 1D model to the photoemission electron spectroscopy data [17,18].

Photoemission from single-crystal surfaces can be modeled as a transition process of an electron between an initial bulk or surface state (ss) inside the lattice with wave function ϕ_i to a time-reversed LEED-like free electron state in vacuum with wave function ϕ_f under the influence of incident light [1,22–24]. The total transition rate of this process is given by Fermi's golden rule as

$$R = \sum_i \sum_f \frac{4\pi}{\hbar}|\langle\phi_f|\mathcal{H}|\phi_i\rangle|^2 \delta[E_f - (E_i + \hbar\omega)] f(E_i), \tag{5}$$

where the summations are over all possible initial and final states (E_i and E_f are the energies of the initial and final states, respectively), the δ function enforces the conservation of energy, and $f(E_i) = [1 + \exp(\frac{E_i}{k_B T})]^{-1}$ is the Fermi-Dirac distribution. k_B is the Boltzmann constant and T is the temperature of the lattice. Note that we have assumed the Fermi level to be 0. The expression for the transition rate includes a factor of 2 to account for the two possible electron spins.

We work within the box approximation to assume that the volume under consideration extends from $-L/2$ to $L/2$ in all directions and $L \to \infty$. Within this assumption we can convert the summations in Eq. (5) to integrals and rewrite the transition rate as

$$R = \frac{4\pi}{\hbar}\left(\frac{L}{2\pi}\right)^6 \int d^3\vec{k}_i \int d^3\vec{k} M^2 \delta[E_f - (E_i + \hbar\omega)] f(E_i), \tag{6}$$

where $M = |\langle\phi_f|\mathcal{H}|\phi_i\rangle|$ is the overlap integral or the matrix element. $\vec{k}_i = k_{ix}\hat{x} + k_{iy}\hat{y} + k_{iz}\hat{z}$ is the wave vector of electrons in their initial state and $\vec{k} = k_x\hat{x} + k_y\hat{y} + k_z\hat{z}$ is the wave vector of the emitted electron. If the work function of the emission surface is W, the energy of the final state, E_f, can be written as

$$E_f = \frac{\hbar^2 k_z^2}{2m_e} + \frac{\hbar^2 k_r^2}{2m_e} + W, \tag{7}$$

where $k_r = \sqrt{k_x^2 + k_y^2}$ is the wave number of the emitted electron in the transverse direction (x-y plane). The delta function in Eq. (6) can then be written as

$$\delta[E_f - (E_i + \hbar\omega)] = \frac{\sqrt{m_e}}{\hbar\sqrt{2X}}\delta(k_z - k_{z0}), \tag{8}$$

where $k_{z0} = \frac{\sqrt{2m_e X}}{\hbar}$, $X = E_i + \hbar\omega - \frac{\hbar^2 k_r^2}{2m_e} - W$. We assume that the electric field in vacuum is small enough that it has no significant impact on the barrier and that the system is in the steady state. Hence the assumption of a step barrier with height W at the solid-vacuum interface is valid.

The QE can simply be calculated as

$$\mathrm{QE} = \frac{R}{FL^2}. \tag{9}$$

As will be shown in the following section, the QE is independent of L as the matrix element is proportional to $1/L^2$ owing to the normalization of the wave functions within the bounding box.

The transverse momentum spread or the rms transverse momentum can be calculated as

$$\sqrt{\langle p_r^2 \rangle} = \left[\frac{\int d^3k_i \int d^3k_f \hbar^2 k_r^2 M^2 \delta[E_f - (E_i + \hbar\omega)] f(E_i)}{\int d^3k_i \int d^3k_f M^2 \delta[E_f - (E_i + \hbar\omega)] f(E_i)} \right]^{1/2}. \tag{10}$$

One can obtain the QE and the rms transverse momentum by calculating the matrix elements M and evaluating the integrals in Eq. (6). Calculation of the matrix elements cannot be generalized further and requires the knowledge of the band structure, wave functions, and the orientation of the photoemitting surface. In the next section, we calculate the matrix elements and perform the integrals to obtain the QE and the rms transverse momentum for the Ag(111) surface as an example.

Here, we would like to note that this model is based on the single independent electron picture of photoemission and does not include many body effects. For low kinetic energy (<1 eV) electrons, image charge potentials of the single emitted electrons and the break down of the sudden approximation may become significant. These effects have been ignored in our model. Despite these, the model is successful at explaining the QE from the Ag(111) surface.

B. Refraction of light at the solid-vacuum interface

In order to calculate the matrix elements, one needs to obtain the polarization vector ($\vec{\epsilon}$) for incident light inside the solid surface. Expressions to obtain $\vec{\epsilon}$ are briefly summarized [25].

We assume the x-z plane to be the plane of incidence. The complex angle of transmission is given by Snell's law as

$$\theta_t = \arcsin\left(\frac{1}{n}\sin(\theta_i)\right), \tag{11}$$

where $n = n_r + in_i$ is the complex index of refraction and θ_i is the angle of incidence.

The angle of the light wave vector inside the metal with respect to the z axis can be given by

$$\theta_t' = \arctan\left[\frac{\sin\theta_i}{q(n_r\cos\gamma - n_i\sin\gamma)}\right] \tag{12}$$

and the optical decay length for the fields can be given by

$$d_l = \frac{c}{\omega q(n_i\cos\gamma + n_r\sin\gamma)}, \tag{13}$$

where

$$q = \left\{ \left[1 - \frac{n_r^2 - n_i^2}{(n_r^2 + n_i^2)^2}\sin^2\theta_i\right]^2 + \left[\frac{2n_r n_i}{(n_r^2 + n_i^2)^2}\sin^2\theta_i\right]^2 \right\}^{1/4} \tag{14}$$

and

$$\gamma = \frac{1}{2}\arctan\frac{2n_r n_i \sin^2\theta_i}{(n_r^2 + n_i^2)^2 - (n_r^2 - n_i^2)\sin^2\theta_i}. \tag{15}$$

For p-polarized light the polarization vector of the vector potential is

$$\vec{\epsilon} = T_p \sin\theta_t \hat{z} + T_p \cos\theta_t \hat{x}, \tag{16}$$

where

$$T_p = \frac{2\cos\theta_i}{\cos\theta_t + n\cos\theta_i}. \tag{17}$$

For s-polarized light the polarization vector of the vector potential is

$$\vec{\epsilon} = T_s \hat{y}, \tag{18}$$

where

$$T_s = \frac{2\cos\theta_i}{n\cos\theta_t + \cos\theta_i}. \tag{19}$$

III. PHOTOEMISSION FROM Ag(111)

In this section, we demonstrate the use of the formalism developed above to obtain analytic expressions for the QE and rms transverse momentum from a Ag(111) surface. The calculated QE matches the experimental values showing the effectiveness of the formalism developed above.

A. Band structure of Ag(111)

We use a two-band fit to the nearly-free-electron-like Ag sp band dispersion model around the L point [26]. The total energy ($E_{i,f}$) can be divided into the longitudinal part ($E_{zi,zf}$) and the transverse part ($E_{ri,rf}$) and can be written as

$$E_{i,f} = E_{zi,zf} + E_{ri,rf}. \tag{20}$$

1. Band structure of bulk states

Within the framework of the nearly-free-electron model, the dispersion relations for the two bands in the longitudinal direction ([111] or z direction) are given by [27]

$$E_{zi,zf} = E_v + V + \frac{\hbar^2 k_{zi,zf}^2}{2m_{i,f}} \mp \left(\frac{\hbar^4 p^2 k_{zi,zf}^2}{m_{i,f}^2} + V^2\right)^{1/2}, \tag{21}$$

where $E_{zi,zf}$ are the longitudinal energies of the electrons in the lower and upper sp bands, respectively, E_v is the valance band maximum, V is the absolute value of the pseudopotential form factor and equals one-half of the gap at the zone boundary, p is the magnitude of the wave vector at L point and is equal to $\frac{\sqrt{3}\pi}{a}$ (a being the lattice constant), and $m_{i,f}$ are the effective mass parameters of the lower and upper sp bands, respectively. It should be noted that $m_{i,f}$ represent higher order corrections from multiband effects and do not correspond to the curvature of the dispersion relations. The subscripts i and f represent the lower and upper sp bands, respectively. The Fermi level is assumed to be 0. The scale for $k_{zi,zf}$ is chosen such that the zero lies at the L point.

The dispersion relation in the transverse directions (x-y plane) is assumed to be cylindrically symmetric and can be

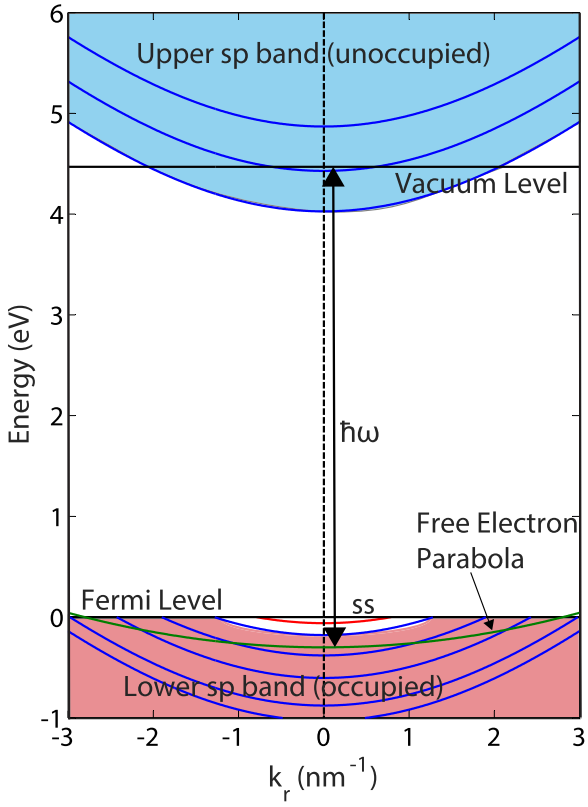

FIG. 1. Band structure of Ag (within the nearly-free-electron model) projected onto the [111] direction. The pink shaded region is the lower sp bands filled with electrons. The region shaded in blue is the upper sp bands, which is unoccupied. The solid red line is the surface state (ss). The solid blue curves are contours of constant $E_{zi,zf}$ or correspondingly constant $k_{zi,zf}$. The green curve is the "free electron parabola" corresponding to a photon energy of $\hbar\omega$. The conservation of energy and transverse momentum allow only the occupied states above this parabola to be emitted.

modeled by nearly parabolic bands given by

$$E_{ri,rf} = \frac{\hbar^2 k_{ri,rf}^2}{2m_{ri,rf}} + \sum_{n=3}^{6} \eta_{ni,nf} k_{ri,rf}^n, \tag{22}$$

where $E_{ri,rf}$ are the transverse energies of the electrons in the lower and upper sp bands, respectively, and $k_{ri,rf}^2 = k_{xi,xf}^2 + k_{yi,yf}^2$ and $m_{ri,rf}$ are the transverse effective masses of the lower and upper sp bands, respectively. The coefficients $\eta_{ni,nf}$ are higher order correction coefficients obtained by fitting the band structure of silver [28].

Figure 1 shows the band structure of Ag projected along the [111] direction. The pink shaded region is the lower sp bands filled with electrons. The states of this band that extend beyond the Fermi level are unoccupied and not shown. The region shaded in blue is the upper sp bands, which is unoccupied. The solid blue curves are contours of constant $E_{zi,zf}$ or correspondingly constant $k_{zi,zf}$. The shape of these contours is nearly parabolic and given by Eq. (22) with an offset of $E_{zi,zf}$.

Values of all parameters used for modeling the bulk band structure are given in Table I and were obtained by fitting the band structure of silver [28].

2. Band structure of surface state

Ag(111) exhibits a Shockley surface state [19] within the band gap at the L point with energy E_s. The surface state has $E_{zi} = E_s$. Since the surface state is located within the band gap, k_{zi} obtained from Eq. (21) is imaginary for the surface state [29]. The dispersion relation in the transverse direction is parabolic and given by

$$E_{ri} = \frac{\hbar^2 k_{ri}^2}{2m_s}. \tag{23}$$

The effective mass of the surface state has been measured to be $m_s = 0.40m_e$ [30]. The energy of the surface state E_s can change significantly with the sample and surface preparation methods and is sensitive to the strain in the crystal. At room temperature it has been reported to range between -20 meV and -120 meV [31,32]. Here, we use it as a fitting parameter and obtain the best fit for QE at $E_s = -100$ meV. This is significantly higher than the most commonly accepted value of ~ -60 meV [33,34], but still lies within the range of measured values previously reported in the literature.

B. Wave functions

Close to the L point, the x and y dependent parts of the initial and final wave functions can be expressed as plane waves. Thus the initial and final wave functions can be expanded as $\phi_i = \phi_{zi} e^{ik_{xi}x} e^{ik_{yi}y}$ and $\phi_f = \phi_{zf} e^{ik_{xf}x} e^{ik_{yf}y}$, respectively. In order to match the transverse part of the final wave functions at the boundary we require $k_{xf} = k_x$ and $k_{yf} = k_y$. Below we give the z dependent parts of the wave functions.

1. Initial bulk states

The z dependent part of the initial wave functions for the bulk states inside the Ag(111) surface can be given by the combination of two Bloch states ($k_{zi} + p$ and $k_{zi} - p$) of the lower sp band and outside the surface can be given by an exponential decay [27]. Thus for $z < z_0$

$$\phi_{zi} = N\{e^{i(k_{zi}+p)z} + \psi_i e^{i(k_{zi}-p)z} + c_1[e^{-i(k_{zi}+p)z} + \psi_i e^{-i(k_{zi}-p)z}]\}, \tag{24}$$

and for $z \geqslant z_0$

$$\phi_{zi} = N c_2 e^{-\kappa_i z'}, \tag{25}$$

where $\kappa_i = \sqrt{2m_e(W - E_{zi})}/\hbar$.

The normalization constant N can be obtained by normalizing the wave function. Constants c_1 and c_2 are obtained by matching the wave function and its derivative at $z = z_0$. The expressions for ψ_i, N, c_1, and c_2 are given in the Appendix.

2. Initial surface states

For the surface state $E_{zi} = E_s$, $k_{zi} = k_{zs}$, $\phi_{zi} = \phi_{zs}$, and $\psi_i = \psi_s$. The energy of the surface state (E_s) lies within the L gap. Hence, from Eq. (21) we see that the value of k_{zs} is imaginary causing the surface state to decay into the bulk.

We can define a decay length for this wave function as $d_w = 1/|k_{zs}|$. In this work, the value of d_w has been calculated to be 2.1 nm using the dispersion relation in Eq. (21). This is close to the value obtained experimentally by perturbing the wave function of the surface state [35]. However, recently, *ab initio* fits to the resonances of the surface state photoemission

TABLE I. List of symbols and values used to model the band structure of the Ag(111) surface.

Symbol	Description	Value
m_i	Longitudinal effective mass parameter of the lower sp band	$0.80m_e$
m_f	Longitudinal effective mass parameter of the upper sp band	$0.90m_e$
m_{ri}	Transverse effective mass of the lower sp band	$0.35m_e$
m_{rf}	Transverse effective mass of the upper sp band	$2.60m_e$
m_s	Effective mass of the surface state	$0.40m_e$
η_{3i}	Third order correction coefficient for the lower sp band	-0.8×10^{-3} eV nm^3
η_{4i}	Fourth order correction coefficient for the lower sp band	-1.0×10^{-3} eV nm^4
η_{5i}	Fifth order correction coefficient for the lower sp band	-3.5×10^{-5} eV nm^5
η_{6i}	Sixth order correction coefficient for the lower sp band	12.5×10^{-6} eV nm^6
η_{3f}	Third order correction coefficient for the upper sp band	2.2×10^{-3} eV nm^3
η_{4f}	Fourth order correction coefficient for the upper sp band	-6.5×10^{-4} eV nm^4
η_{5f}	Fifth order correction coefficient for the upper sp band	-5.6×10^{-5} eV nm^5
η_{6f}	Sixth order correction coefficient for the upper sp band	20.8×10^{-6} eV nm^6
E_s	Energy of the surface state	-100 meV
E_v	Valance band maximum at the L point	-178 meV
V	Pseudopotential form factor (equals one-half band gap at the L point)	2.1 eV
W	Work function of Ag(111)	4.45 eV
a	Unit cell length	0.409 nm

peak have suggested nearly a factor of 3 smaller value of this decay length [36]. We find that the QE is insensitive to the decay length and varies by only 20% for large (factor of 3) changes in the decay length of the wave function.

For $z < z_0$ the wave function of the ss is given by

$$\phi_{zs} = N_s[e^{i(k_{zs}+p)z} + \psi_s e^{i(k_{zs}-p)z}], \tag{26}$$

and for $z > z_0$ it is given by

$$\phi_{zs} = N_s c_s e^{-\kappa_s z'}, \tag{27}$$

where $\kappa_s = \sqrt{2m_e(W-E_s)}/\hbar$. N_s is the normalization constant and can be obtained by normalizing the wave function. c_s and z_0 can be obtained by matching the wave function and its derivative at $z = z_0$. Expressions for N_s and c_s are given in the Appendix. An explicit expression cannot be obtained for z_0 and its value needs to be calculated numerically to satisfy the continuity conditions of the wave functions as given in the Appendix.

3. *Final states*

The final state wave functions are not the free electron wave functions of the emitted electron, but are time-reversed LEED states as required by the one-step photoemission theory [1,24]. Inside the Ag(111) surface they can be given by the combination of two Bloch states ($k_{zi} + p$ and $k_{zi} - p$) of the upper sp band along with an exponential decay to account for the various scattering mechanisms that prevent emission of excited electrons. The final wave functions outside the surface are plane waves. Thus for $z < z_0$

$$\phi^*_{zf} = t^*_{pk}\{e^{[-i(k_{zf}+p)+k_d]z} + \psi_f e^{[-i(k_{zf}-p)+k_d]z}\}\sqrt{\frac{2}{L}}, \tag{28}$$

where $k_d = s/d_{e\text{-}e}$ is the exponential decay constant that takes into account the scattering mechanisms that prevent emission of excited electrons. $d_{e\text{-}e}$ is the electron-electron scattering length, which is the dominant scattering mechanism in metals. The scattering parameter s is used as a fitting parameter in the calculation.

For $z \geqslant z_0$

$$\phi^*_{zf} = [e^{-ik_z z'} + r^*_{pk} e^{ik_z z'}]\sqrt{\frac{2}{L}}, \tag{29}$$

where $\hbar k_z = \sqrt{2m_e(E_{fz} - W)}$ is the momentum of the emitted electron in the z direction. Constants t^*_{pk} and r^*_{pk} are obtained by matching the wave function and its derivative at $z = z_0$. Expressions for ψ_f, t^*_{pk}, and r^*_{pk} are given in the Appendix. Note that the normalization of the final states is such that the outgoing plane wave representing the emitted photoelectron is normalized to unity.

Figure 2 shows an example of the real component of the z dependent part of the initial bulk, surface, and final wave functions.

C. Calculation of the matrix elements

For p-polarized light, using the Hamiltonian from Eq. (4), the matrix elements $M = |\langle\phi_f|\mathcal{H}|\phi_i\rangle|$ from Eq. (6) can be written as

$$M = \frac{e\hbar|A_0 T_p|}{m_e c} \times \left|\langle\phi_{f1}|\sin\theta_t\frac{\partial}{\partial z} + \cos\theta_t\frac{\partial}{\partial x} + \sin\theta_t C\delta(z')|\phi_i\rangle\right|, \tag{30}$$

where $\phi_{f1} = \phi_f e^{z'H(-z')/d_l}$.

Using the wave functions given in the previous section and integrating over the box one can calculate M^2 for p-polarized light as

$$M^2 = \frac{4K_1|T_p|^2}{L^4}k_z^2|(I_d + CI_s)\sin\theta_t + ik_{xi}I\cos\theta_t|^2 \times h(k_{xi} - k_{xf})h(k_{yi} - k_{yf}), \tag{31}$$

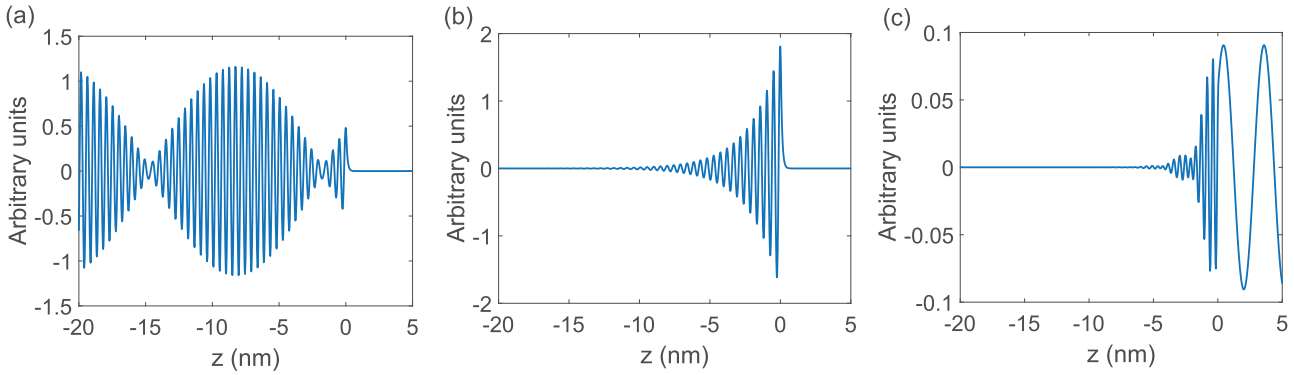

FIG. 2. Example of the real component of the z dependent part of the initial bulk (a), surface (b), and final (c) wave functions. Here $z_0 = 0.042$ nm and $s = 12.5$.

where $K_1 = \frac{e^2\hbar^2|A_0|^2}{m_e^2c^2}$ and $h(\zeta) = \frac{1}{L}[\frac{2\sin(L\zeta/2)}{\zeta}]^2$. Note that in the limit $L \to \infty$, $h(\zeta) = 2\pi\delta(\zeta)$. I_d, I_s, and I are given as follows:

$$I_d = \frac{L/2}{k_z}\int_{-L/2}^{L/2} dz\, \phi_{zf}^* e^{[z'H(-z'')d_l]}\frac{\partial}{\partial z}\phi_{zi}, \tag{32}$$

$$I_s = \frac{L/2}{k_z}\phi_{zf}^*(z_0)\phi_{zi}(z_0), \tag{33}$$

$$I = \frac{L/2}{k_z}\int_{-L/2}^{L/2} dz\, \phi_{zf}^* e^{[z'H(-z')/d_l]}\phi_{zi}. \tag{34}$$

The integrals I_d and I can be evaluated analytically and the expressions are given in the Appendix. Owing to the appropriate normalization of the wave functions, I_d, I_s, and I are independent of L when $L \to \infty$.

Note that the matrix element given in Eq. (31) is asymmetric in k_{xi}. This can lead to an asymmetric photoemission where the number of electrons emitted with momentum k_x is different from electrons with number of electrons with x direction momentum $-k_x$.

The matrix element for s-polarized light can be given by

$$M^2 = \frac{4K_1|T_s|^2}{L^4}k_z^2|ik_{yi}I|^2 h(k_{xi}-k_{xf})h(k_{yi}-k_{yf}). \tag{35}$$

D. Calculating the QE

The total QE can be written as the sum of the QE contribution from the bulk states ($\mathrm{QE_{bulk}}$) and the surface state ($\mathrm{QE_{ss}}$):

$$\mathrm{QE} = \mathrm{QE_{bulk}} + \mathrm{QE_{ss}}. \tag{36}$$

$\mathrm{QE_{bulk}}$ can be given by

$$\mathrm{QE_{bulk}} = \frac{R_{\mathrm{bulk}}}{FL^2}, \tag{37}$$

where R_{bulk} can be calculated from Eq. (6) with the integrations being carried over all possible initial bulk and final states. F is the incident photon flux per unit area given by Eq. (3).

$\mathrm{QE_{ss}}$ can be given by

$$\mathrm{QE_{ss}} = \frac{R_{\mathrm{ss}}}{FL^2}. \tag{38}$$

R_{ss} can be calculated by an expression similar to Eq. (6) with the difference that the integration over the initial state has to be performed over k_{xi} and k_{yi} only, due to the two-dimensional nature of the surface state. R_{ss} can be written as

$$R_{\mathrm{ss}} = \frac{4\pi}{\hbar}\left(\frac{L}{2\pi}\right)^5\int\int dk_{xi}dk_{yi} \times \int d^3\vec{k}\, M^2\delta[E_f - (E_i + \hbar\omega)]f(E_i). \tag{39}$$

Using Eqs. (3), (6), (8), (31), and (37), $\mathrm{QE_{bulk}}$ for p-polarized light can be written as

$$\mathrm{QE_{bulk}} = \frac{K}{(2\pi)^2}\int d^3\vec{k}_i\int d^3\vec{k}\frac{k_z^2}{k_{z0}}|(I_d + CI_s)\sin\theta_t + ik_{xi}I\cos\theta_t|^2 h(k_{xi}-k_x)h(k_{yi}-k_y) \times \delta(k_z - k_{z0})f(E_i), \tag{40}$$

where $K = \frac{8(\hbar c)^2\alpha|T_p|^2}{(2\pi)^2(m_ec^2)\hbar\omega}$ and α is the fine structure constant. Note that we require $k_{xf} = k_x$ and $k_{yf} = k_y$ in order to match the transverse part of the final wave functions at the boundary.

In the limit as $L \to \infty$, $h(\zeta) = 2\pi\delta(\zeta)$. Taking the limit as $L \to \infty$ and integrating over the final states we obtain

$$\mathrm{QE_{bulk}} = K\int d^3\vec{k}_i k_{z0}|(I_d + CI_s)\sin\theta_t + ik_{xi}I\cos\theta_t|^2 f(E_i). \tag{41}$$

Note that I, I_d, I_s, k_z0, and E_i are functions of $\vec{k}_i$ and $\vec{k}$. Integrating the δ functions in Eq. (40) we get $k_x = k_{xi}$, $k_y = k_{yi}$, and $k_z = k_{z0}$. These δ functions enforce the conservation of transverse momentum and energy during photoemission.

Similarly, $\mathrm{QE_{ss}}$ can be obtained using Eq. (38) as

$$\mathrm{QE_{ss}} = \frac{2\pi K}{L}\int dk_{xi}\int dk_{yi}k_{z0}|(I_d + CI_s)\sin\theta_t + ik_{xi}I\cos\theta_t|^2 f(E_i). \tag{42}$$

The normalization constant for the surface state (N_s) is not dependent on L. Hence, for the surface state I, I_d and I_s are proportional to $\sqrt{L}$ even as $L \to \infty$. Thus, the surface state QE as given in Eq. (42) remains independent of L as $L \to \infty$.

After writing k_{xi} and k_{yi} in cylindrical coordinates as $k_{xi} = k_r\cos\varphi$ and $k_{xi} = k_r\sin\varphi$, then integrating over φ the above

expressions for QE_{bulk} and QE_{ss} can be written as

$$QE_{bulk} = 2\pi K \int dk_r \int dk_{zi} k_r k_{z0} f(E_i) \times \left[|(I_d + CI_s)\sin\theta_t|^2 + k_r^2 \frac{|I\cos\theta_t|^2}{2} \right] \quad (43)$$

and

$$QE_{ss} = \frac{4\pi^2 K}{L} \int dk_r k_r k_{z0} f(E_i) \times \left[|(I_d + CI_s)\sin\theta_t|^2 + k_r^2 \frac{|I\cos\theta_t|^2}{2} \right], \quad (44)$$

respectively.

The QE for s-polarized light can be similarly calculated by using the appropriate matrix elements. The 3D momentum distributions and the rms transverse momentum can also be calculated easily as shown in Eq. (10).

IV. RESULTS AND DISCUSSION

A. Spectral response

Figure 3 compares the spectral response measured from an Ag(111) surface to the result obtained from the photoemission model presented above, for p-polarized light at various angles of incidence.

In order to measure the QE, a commercially bought [37] single-crystal Ag(111) sample was prepared in an ultrahigh vacuum chamber with base pressure in the low 10^{-10} torr range. Several cycles of Ar ion bombardment and annealing to 500 °C were performed until a sharp hexagonal LEED pattern was observed. The surface cleanliness was verified using Auger electron spectroscopy. The QE was obtained by measuring the photocurrent and the power of light incident on the sample surface. A laser based plasma lamp with a monochromator [38] was used as a light source for the QE measurement. The spectral width of the light source was 2 nm FWHM.

All constants used for modeling the band structure to calculate the QE are given in Table I. The optical constants (n_r and n_i) for silver as a function of wavelength are well known

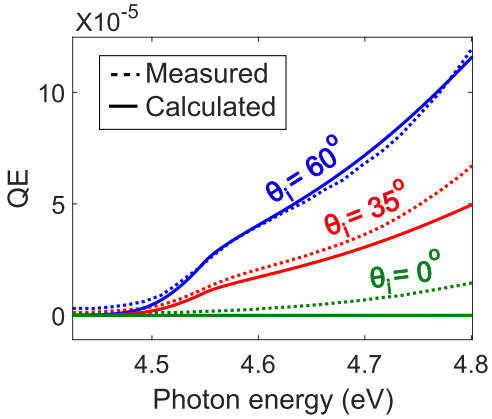

FIG. 3. Measured and calculated spectral response of the Ag(111) surface at various angles of incidence (θ_i) in p-polarized light. The error bar on the experimental measurement is ~10%.

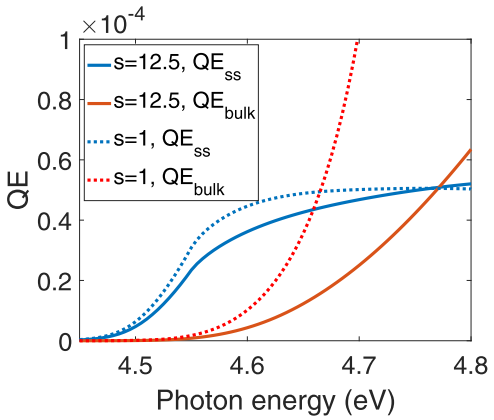

FIG. 4. QE_{bulk} and QE_{ss} for $s = 1$ and $s = 12.5$. QE_{ss} is not very sensitive to s because the surface state electrons are localized at the surface and do not need to travel inside the metal to get emitted.

[39,40]. The surface constant C and the electron-electron scattering length $d_{e\text{-}e}$ were obtained as a function of photon energy by extrapolating the values of C and $d_{e\text{-}e}$ obtained from PES measurements [17,18]. The scattering parameter s is set to 12.5 to obtain a good match to the experimental data.

Figure 3 shows that the calculated QE explains the experimental data, both qualitatively and quantitatively. With the exception of the scattering parameter s, this photoemission model calculates the QE accurately without the use of any *ad hoc* coefficients or scaling factors. It is seen that the QE increases with the angle of incidence for p-polarized light (vectorial photoelectric effect). The knee observed in the spectral response for higher angles of incidence at ~4.55 eV is caused due to the surface state. This becomes clear from Fig. 4, which shows the contributions to the QE from the bulk and surface states. The sections below discuss the effect of the scattering parameter and the vectorial photoelectric effect, respectively.

1. *Effect of scattering*

The decay constant of the final wave function k_d takes into account the electrons that were excited by light but were unable to escape due to various scattering mechanisms while traveling towards the surface. The inelastic electron-electron scattering is the dominant scattering mechanism of excited electrons in metals. Hence we write $k_d = s/d_{e\text{-}e}$, where $d_{e\text{-}e}$ is the electron-electron scattering mean free path and s is adjusted to match the calculated QE to the experimental value. Figure 4 shows QE_{bulk} and QE_{ss} for $s = 1$ and $s = 12.5$. We can see that QE_{ss} does not change significantly with s. The surface state is localized at the metal-vacuum interface. Hence the electrons excited from the surface state do not need to travel inside the metal to get emitted. This causes QE_{ss} to be insensitive to s or k_d.

In order to match the experimental data, s needs to be set to a particularly large value of 12.5. This implies a much higher effective scattering rate than set by the electron-electron scattering lengths obtained from UV-PES data [17,18]. The reason for this increased scattering is not clear.

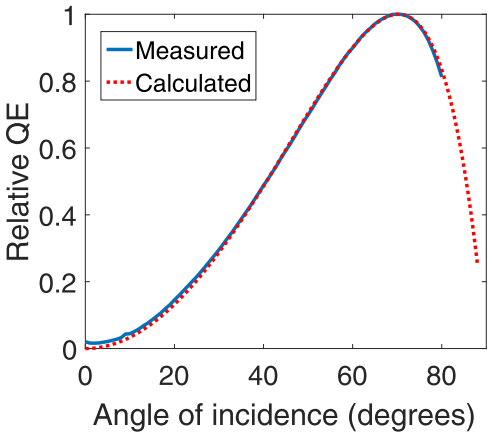

FIG. 5. The theoretical curve for the vectorial photoelectric effect obtained from equation (45) matches the experimental data measured at photon energy of 4.57 eV.

2. *Vectorial photoelectric effect*

Vectorial photoelecric effect is the variation of QE with the angle of incidence and polarization of incident light.

The QE for p-polarized light is given by Eqs. (43) and (44). In these equations, the term $|(I_d + CI_s)\sin\theta_t|^2$ corresponds to the QE contribution of the z component of the polarization vector and the term $k_r^2 \frac{|I\cos\theta_t|^2}{2}$ corresponds to the QE contribution of the x component of the polarization vector. For the band structure and wave functions used here, $|(I_d + CI_s)|^2 \gg k_r^2 \frac{|I|^2}{2}$. As a result, the photoemission from the Ag(111) surface is dominated by the z component of the polarization vector (i.e., component perpendicular to the surface). Neglecting the contribution of the x (parallel to surface) component, the QE can be written as

$$\mathrm{QE} = K_p \frac{|T_p \sin\theta_t|^2}{\cos\theta_i}, \tag{45}$$

where K_p is a constant independent of the angle of incidence. Note that both T_p and θ_t are dependent on the angle of incidence. Figure 5 shows that the experimentally measured angular dependence of QE for p-polarized light matches this calculation. This dependence is similar to the angular dependence of QE measured for several materials [14,15,41,42].

The spectral response calculated by the model at 0° angle of incidence is much smaller than the experimental value (see Fig. 3). At 0° angle of incidence only the x and y components of the polarization vector exist. This implies that the experimentally observed contribution of the x and y components of the polarization vector is larger than that calculated by the model. The assumption that the wave functions in the x and y directions are modeled by plane waves could be one possible culprit for this. Emission from parts of the band structure not modeled by the nearly-free-electron representation, many-body photoemission effects like the hole state lifetime induces energy spread [43], and the breakdown of the sudden approximation [44] are other effects which may be responsible for this discrepancy. They may also be responsible for the large effective scattering parameter.

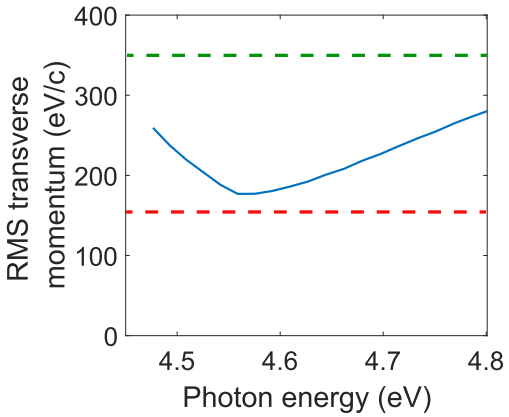

FIG. 6. The blue curve shows the rms transverse momentum calculated for the Ag(111) surface. The dashed green line shows the rms transverse momentum typically obtained from cathodes in the state-of-art electron guns. The red dashed line indicates the thermally limited rms transverse momentum [13]. At 4.57 eV photon energy Ag(111) gives near thermal rms transverse momentum with a QE of 5×10^{-5} making it a much better electron source than the current state-of-the-art.

B. Transverse momentum spread

Figure 6 shows the rms transverse momentum expected from the Ag(111) surface. The rms transverse momentum has been calculated using Eq. (10) for angle of incidence equal to 60°. It can be seen that the rms transvserse momentum initially decreases, reaches a minimum, and then increases with increasing photon energy. At photon energies very close to threshold only electrons from the ring formed by the intersection of the surface state with the Fermi level are emitted. These electrons have a relatively high transverse momentum. At higher photon energies, electrons from the surface state with lower transverse momentum and lower energy can also be emitted along with the electrons from the surface state ring at the Fermi level. This causes the rms transverse momentum to initially reduce with increasing photon energy. This decline continues until the photon energy is sufficiently high to allow emission from the entire surface state. At this photon energy the rms momentum reaches a minimum. At higher photon energies, the electrons from bulk states which are located near the Fermi level and have a much higher transverse momentum are allowed to be emitted causing the rms transverse momentum to increase again.

The smallest rms momentum measured from polycrystalline metal cathodes (which are typically used as electron sources) is limited by the room temperature to a value of 160 eV/c [13] at the photoemission threshold. However, at the photoemission threshold the QE is also very low (in the 10^{-6}–10^{-7}) range making polycrystalline cathodes unusable in this regime. At higher photon energies, the QE increases but so does the rms transverse momentum. In order to obtain a desirable QE greater than 10^{-5} the photon energy used has to be several 100 meV above threshold. This sets the rms transverse momentum practically obtained in electron guns to ∼350 eV/c [12]. According to our calculations, Ag(111) when operated at an angle of incidence of 60° in p-polarized light at 4.57 eV can act as a cathode with rms transverse

momentum lower than 180 eV/c and a QE as high as 5×10^{-5}. This shows that Ag(111) can act as a better photocathode the polycrystalline metals currently used as electron sources.

V. CONCLUSION

We have presented a 3D one-step model that allows us to calculate photoemission properties such as QE and rms transverse momentum of emitted electrons from single-crystal surfaces. Optimizing these photoemission properties can greatly improve the performance of electron source applications such as FELs and UED.

Using the example of photoemission from Ag(111) we show that not only can this model calculate the spectral response from surface state without the use of any *ad hoc* parameters, but also explains the photoemission phenomena of the vectorial photoelectric effect accurately.

We also calculate the rms transverse momentum from an Ag(111) surface and show that in p-polarized light with a high angle of incidence, the Ag(111) surface can exhibit high QE along with a small rms transverse momentum, making it a much better cathode than the currently used polycrystalline metals. Upon integrating with other band structure and wave function calculation techniques like density functional theory, this methodology can be used to calculate the electron source relevant photoemission properties from any single-crystal surface in order to identify ideal electron emitters from first-principles calculations [45]. Such a methodology is essential to screen for materials to identify good electron emitters.

ACKNOWLEDGMENTS

The authors would like to thank Dr. T. Miller for stimulating discussions. This work was supported by the Director, Office of Science, Office of Basic Energy Sciences of the U.S. Department of Energy, under Contracts No. KC0407-ALSJNT-I0013 and No. DE-AC02-05CH11231 (W.W., S.K., J.F., H.A.P.) and the U.S. National Science Foundation under Grant No. DMR 13-05583 (T.-C.C.).

S.K. and W.W. have contributed equally to this work.

APPENDIX

The analytic expressions to calculate several of the coefficients used in the wave function calculations are given below:

$$\psi_{i,f} = \frac{\left(\frac{\hbar^2(k_{zi,zf}+p)^2}{2m_{i,f}} - \frac{\hbar^2 p^2}{2m_{i,f}} - E_{zi,zf} + V + E_v\right)}{V}, \tag{A1}$$

$$c_1 = \frac{[\kappa_i + i(k_{zi}+p)]e^{i(k_{zi}+p)z_0} + [\kappa_i + i(k_{zi}-p)]\psi_i e^{i(k_{zi}-p)z_0}}{[-\kappa_i + i(k_{zi}+p)]e^{-i(k_{zi}+p)z_0} + [-\kappa_i + i(k_{zi}-p)]\psi_i e^{-i(k_{zi}-p)z_0}}, \tag{A2}$$

$$c_2 = 2i\frac{(k_{zi}+p) + (k_{zi}-p)\psi_i^2 + 2k_{zi}\psi_i\cos(2pz_0)}{[\kappa_i + i(k_{zi}+p)]e^{-i(k_{zi}+p)z_0} + [-\kappa_i + i(k_{zi}-p)]e^{-i(k_{zi}-p)z_0}}, \tag{A3}$$

$$t_{pk} = \frac{2ik_z}{[i(k_{zf}+p+k_z)+k_d]e^{[i(k_{zf}+p)+k_d]z_0} + [i(k_{zf}-p+k_z)+k_d]\psi_f e^{[i(k_{zf}-p)+k_d]z_0}}, \tag{A4}$$

$$1 + r_{pk} = \frac{2ik_z[e^{[i(k_{zf}+p)+k_d]z_0} + \psi_f e^{[i(k_{zf}-p)+k_d]z_0}]}{[i(k_{zf}+p+k_z)+k_d]e^{[i(k_{zf}+p)+k_d]z_0} + [i(k_{zf}-p+k_z)+k_d]\psi_f e^{[i(k_{zf}-p)+k_d]z_0}}, \tag{A5}$$

$$N = \frac{\sqrt{(2)}}{\sqrt{\left(\frac{L}{2}\right)(1+\psi_i^2)(1+|c_1|^2)}} \qquad \text{(assuming } L \to \infty\text{)}, \tag{A6}$$

$$c_s = e^{i(k_{zs}+p)z_0} + \psi_s e^{i(k_{zs}-p)z_0}, \tag{A7}$$

$$N_s = \sqrt{(2)}\left\{\frac{e^{2k_{zs}z_0}}{2k_{zs}}(1+|\psi_s|^2) + \mathrm{Re}\left[\psi_s^*\frac{e^{2(ip+k_{zs})}}{ip+k_{zs}}\right] + \frac{|c_s|^2}{2\kappa_s}\right\}^{-1/2}. \tag{A8}$$

Note that the wave functions have been normalized to 2 in order to account for the electrons emitted from the equivalent L point at $(-\frac{\pi}{a}, -\frac{\pi}{a}, -\frac{\pi}{a})$. z_0 can be obtained by solving the following equation numerically:

$$i(k_{zs}+p)e^{i(k_{zs}+p)z_0} + i\psi_s(k_{zs}-p)e^{i(k_{zs}-p)z_0} = -\kappa_s c_s. \tag{A9}$$

The analytic expressions for the integrals I_d and I used in the matrix element calculations are given below:

$$I_d = \int dz\,\phi_{zf}^*\frac{\partial}{\partial z}\phi_{zi} = N\kappa_i c_2\left(\frac{2ik_z}{\kappa_i^2+k_z^2} + \frac{1+r_{pk}^*}{-\kappa_i+ik_z}\right)$$
$$+ Nt_{pk}^*\left[\frac{i(k_{zi}+p)e^{[i(-k_{zf}+k_{zi})+k_d]z_0}}{i(-k_{zf}+k_{zi})+k_d} + \phi_i\frac{i(k_{zi}-p)e^{[i(-k_{zf}+k_{zi}-2p)+k_d]z_0}}{i(-k_{zf}+k_{zi}-2p)+k_d} - c_1\frac{i(k_{zi}+p)e^{[-i(k_{zf}+k_{zi}+2p)+k_d]z_0}}{-i(k_{zf}+k_{zi}+2p)+k_d}\right.$$

$$- c_1\phi_i \frac{i(k_{zi}-p)e^{[-i(k_{zf}+k_{zi})+k_d]z_0}}{-i(k_{zf}+k_{zi})+k_d} + \phi_f \frac{i(k_{zi}+p)e^{[i(-k_{zf}+k_{zi}+2p)+k_d]z_0}}{i(-k_{zf}+k_{zi}+2p)+k_d} + \phi_i\phi_f \frac{i(k_{zi}-p)e^{[i(-k_{zf}+k_{zi})+k_d]z_0}}{i(-k_{zf}+k_{zi})+k_d}$$
$$- c_1\phi_f \frac{i(k_{zi}+p)e^{[-i(k_{zf}+k_{zi})+k_d]z_0}}{-i(k_{zf}+k_{zi})+k_d} - c_1\phi_i \frac{i(k_{zi}-p)e^{[-i(k_{zf}+k_{zi}-2p)+k_d]z_0}}{-i(k_{zf}+k_{zi}-2p)+k_d}\Bigg], \tag{A10}$$

$$I = \int dz\, \phi^*_{zf}\phi_{zi} = Nc_2\left(\frac{2ik_z}{\kappa_i^2+k_z^2} + \frac{1+r^*_{pk}}{-\kappa_i+ik_z}\right) + Nt^*_{pk}\Bigg[\frac{e^{[i(-k_{zf}+k_{zi})+k_d]z_0}}{i(-k_{zf}+k_{zi})+k_d} + \phi_i \frac{e^{[i(-k_{zf}+k_{zi}-2p)+k_d]z_0}}{i(-k_{zf}+k_{zi}-2p)+k_d}$$
$$- c_1 \frac{e^{[-i(k_{zf}+k_{zi}+2p)+k_d]z_0}}{-i(k_{zf}+k_{zi}+2p)+k_d} - c_1\phi_i \frac{e^{[-i(k_{zf}+k_{zi})+k_d]z_0}}{-i(k_{zf}+k_{zi})+k_d} + \phi_f \frac{e^{[i(-k_{zf}+k_{zi}+2p)+k_d]z_0}}{i(-k_{zf}+k_{zi}+2p)+k_d}$$
$$+ \phi_i\phi_f \frac{e^{[i(-k_{zf}+k_{zi})+k_d]z_0}}{i(-k_{zf}+k_{zi})+k_d} - c_1\phi_f \frac{e^{[-i(k_{zf}+k_{zi})+k_d]z_0}}{-i(k_{zf}+k_{zi})+k_d} - c_1\phi_i \frac{e^{[-i(k_{zf}+k_{zi}-2p)+k_d]z_0}}{-i(k_{zf}+k_{zi}-2p)+k_d}\Bigg]. \tag{A11}$$

[1] S. D. Kevan and W. Eberhardt, in *Angle Resolved Photoemission: Theory and Current Applications*, edited by S. D. Kevan (Elsevier, Amsterdam, 1992).
[2] P. Emma, R. Akre, J. Arthur, R. Bionta, C. Bostedt, J. Bozek, A. Brachmann, P. Bucksbaum, R. Coffee, F. Decker *et al.*, Nat. Photon. **4**, 641 (2010).
[3] A. H. Zewail, Annu. Rev. Phys. Chem. **57**, 65 (2006).
[4] D. Dowell, I. Bazarov, B. Dunham, K. Harkay, C. Hernandez-Garcia, R. Legge, H. Padmore, T. Rao, J. Smedley, and W. Wan, Nucl. Instrum. Methods, Phys. Res., Sect. A **622**, 685 (2010).
[5] S. Karkare, L. Boulet, L. Cultrera, B. Dunham, X. Liu, W. Schaff, and I. Bazarov, Phys. Rev. Lett. **112**, 097601 (2014).
[6] P. Schmüser, M. Dohlus, and J. Rossbach, *Ultraviolet and Soft X-Ray Free-Electron Lasers* (Springer, Berlin/Heidelberg, 2009).
[7] D. H. Dowell, J. Castro, P. Emma, J. Frisch, S. Gilevich, G. Hays, P. Hering, C. Limborg-Deprey, H. Loos, A. Miahnahri, and W. White, in *2007 IEEE Particle Accelerator Conference (PAC)*, 2007 (unpublished), pp. 1317–1319.
[8] J. Maxson, P. Musumeci, L. Cultrera, S. Karkare, and H. Padmore, Nucl. Instrum. Methods Phys. Res., Sect. A (2016), doi:10.1016/j.nima.2016.08.032.
[9] C. N. Berglund and W. E. Spicer, Phys. Rev. **136**, A1030 (1964).
[10] K. Flottmann, TESLA FEL Reports, 1997-01, https://flash.desy.de/sites2009/site_vuvfel/content/e403/e1642/e839/e829/infoboxContent830/tesla-fel1997-01.pdf
[11] K. L. Jensen, P. G. O'Shea, D. W. Feldman, and N. A. Moody, Appl. Phys. Lett. **89**, 224103 (2006).
[12] D. H. Dowell and J. F. Schmerge, Phys. Rev. ST Accel. Beams **12**, 074201 (2009).
[13] J. Feng, J. Nasiatka, W. Wan, S. Karkare, J. Smedley, and H. Padmore, Appl. Phys. Lett. **107**, 134101 (2015).
[14] R. M. Broudy, Phys. Rev. B **3**, 3641(1971).
[15] E. Pedersoli *et al.*, Appl. Phys. Lett. **93**, 183505 (2008).
[16] T. Li, L. Rickman, and W. A. Schroeder, J. Appl. Phys. **117**, 134901 (2015).
[17] T. Miller, W. E. McMahon, and T.-C. Chiang, Phys. Rev. Lett. **77**, 1167 (1996).
[18] T. Miller, E. D. Hansen, W. E. McMahon, and T.-C. Chiang, Surf. Sci. **376**, 32 (1997).
[19] W. Shockley, Phys. Rev. **56**, 317 (1939).
[20] Note that calculating the absolute value of the QE still requires the use of some empirical data.
[21] J. J. Sakurai, *Modern Quantum Mechanics* (Addison-Wesley, Melno Park, CA, 1994).
[22] I. Adawi, Phys. Rev. **134**, A788 (1964).
[23] E. O. Kane, Phys. Rev. **127**, 131 (1962).
[24] G. D. Mahan, Phys. Rev. B **2**, 4334 (1970).
[25] M. Born and E. Wolf, *Principles of Optics* (Pergamon, Oxford, 1970).
[26] N. V. Smith, Phys. Rev. B **32**, 3549 (1985).
[27] T.-C. Chiang, Surf. Sci. Rep. **39**, 181 (2000).
[28] A. Goldmann, *Landolt-Börnstein Numerical Data and Functional Relationships in Science and Technology* (Springer-Verlag, Berlin, 2003), Chap. 2.9.3, p. 51.
[29] S. Hufner, *Photoelectron Spectroscopy: Principles and Applications* (Springer, Berlin/Heidelberg, 2003).
[30] F. Reinert, G. Nicolay, S. Schmidt, D. Ehm, and S. Hufner, Phys. Rev. B **63**, 115415 (2001).
[31] S. D. Kevan and R. H. Gaylord, Phys. Rev. B **36**, 5809 (1987).
[32] R. Paniag, R. Matzdorf, G. Meister, and A. Goldmann, Surf. Sci. **336**, 113 (1995).
[33] V. M. Silkin, P. Lazic, N. Doslic, H. Petek, and B. Gumhalter, Phys. Rev. B **92**, 155405 (2015).
[34] X. Cui, C. Wang, A. Argondizzo, S. Garrett-Roe, B. Gumhalter, and H. Petek, Nat. Phys. **10**, 505 (2014).
[35] T. C. Hsieh, T. Miller, and T. C. Chiang, Phys. Rev. Lett. **55**, 2483 (1985).
[36] J. Lobo-Checa, J. E. Ortega, A. Mascaraque, E. G. Michel, and E. E. Krasovskii, Phys. Rev. B **84**, 245419 (2011).
[37] Surface preparation laboratories, https://www.spl.eu/
[38] J. Feng, J. Nasiatka, J. Wong, X. Chen, S. Hidalgo, T. Vecchione, H. Zhu, F. J. Palomares, and H. A. Padmore, Rev. Sci. Instrum. **84**, 085114 (2013).
[39] K. Stahrenberg, T. Herrmann, K. Wilmers, N. Esser, W. Richter, and M. J. G. Lee, Phys. Rev. B **64**, 115111 (2001).
[40] Refractive index database, http://refractiveindex.info/
[41] G. V. Benemanskaya, M. N. Lapushkin, Y. N. Gnedin, and G. W. Fraser, Il Nuovo Cimento D **16**, 599 (1994).
[42] D. W. Juenker, J. P. Waldron, and R. J. Jaccodine, J. Opt. Soc. Am. **54**, 216 (1964).
[43] A. Eiguren, B. Hellsing, F. Reinert, G. Nicolay, E. V. Chulkov, V. M. Silkin, S. Hufner, and P. M. Echenique, Phys. Rev. Lett. **88**, 066805 (2002).
[44] A. Tamai, W. Meevasana, P. D. C. King, C. W. Nicholson, A. de la Torre, E. Rozbicki, and F. Baumberger, Phys. Rev. B **87**, 075113 (2013).
[45] B. Camino, T. Noakes, M. Surman, E. Seddon, and N. Harrison, Comput. Mater. Sci. **122**, 331 (2016).